A&A 563, L5 (2014)
DOI: 10.1051/0004-6361/201323212

Astronomy & Astrophysics

Letter to the Editor

The lead discrepancy in intrinsically *s*-process enriched post-AGB stars in the Magellanic Clouds⋆

K. De Smedt[1], H. Van Winckel[1], D. Kamath[1], A. I. Karakas[2], L. Siess[3], S. Goriely[3], and P. Wood[3]

[1] Instituut voor Sterrenkunde, K.U. Leuven, Celestijnenlaan 200B, 3001 Leuven, Belgium
e-mail: kenneth.desmedt@ster.kuleuven.be
[2] Research School of Astronomy and Astrophysics, Mount Stromlo Observatory, ACT 2611 Weston Creek, Australia
[3] Institut d'Astronomie et d'Astrophysique, Université Libre de Bruxelles, ULB, CP 226, 1050 Brussels, Belgium

Received 7 December 2013 / Accepted 9 February 2014

ABSTRACT

Context. Our understanding of the *s*-process nucleosynthesis in asymptotic giant branch (AGB) stars is incomplete. AGB models predict, for example, large overabundances of lead (Pb) compared to other *s*-process elements in metal-poor low-mass AGB stars. This is indeed observed in some extrinsically enhanced metal-poor stars, but not in all. An extensive study of intrinsically *s*-process enriched objects is essential for improving our knowledge of the AGB third dredge-up and associated *s*-process nucleosynthesis.
Aims. We compare the spectral abundance analysis of the SMC post-AGB star J004441.04-732136.4 with state-of-the-art AGB model predictions with a main focus on Pb. The low signal-to-noise (S/N) in the Pb line region made the result of our previous study inconclusive. We acquired additional data covering the region of the strongest Pb line.
Methods. By carefully complementing re-reduced previous data, with newly acquired UVES optical spectra, we improve the S/N of the spectrum around the strongest Pb line. Therefore, an upper limit for the Pb abundance is estimated from a merged weighted mean spectrum using synthetic spectral modeling. We then compare the abundance results from the combined spectra to predictions of tailored AGB evolutionary models from two independent evolution codes. In addition, we determine upper limits for Pb abundances for three previously studied LMC post-AGB objects.
Results. Although theoretical predictions for J004441.04-732136.4 match the *s*-process distribution up to tungsten (W), the predicted very high Pb abundance is clearly not detected. The three additional LMC post-AGB stars show a similar lack of a very high Pb abundance.
Conclusions. From our study, we conclude that none of these low-mass, low-metallicity post-AGB stars of the LMC and SMC are strong Pb producers. This conflicts with current theoretical predictions.

Key words. stars: AGB and post-AGB – stars: evolution – stars: abundances – Magellanic Clouds – stars: chemically peculiar

1. Introduction

During the asymptotic giant branch (AGB), stars undergo thermal pulses that may be followed by third dredge-ups during which freshly synthesized products are brought into the envelope, among them the carbon and *s*-process elements. Theoretical and observational evidence shows that the main neutron source in low-mass AGB stars (1−3 $M_{\odot}$) is the $^{13}C(\alpha, n)^{16}O$ reaction (Straniero et al. 1995; Gallino et al. 1998; Abia et al. 2002). It is widely accepted that the ^{13}C pocket originates in a region where protons from the H-rich convective envelope are mixed into the He-rich intershell after a thermal pulse. However, the physical mechanisms of both third dredge-up and partial mixing in the intershell remain poorly understood.

The *s*-process nucleosynthesis is predicted to depend strongly on metallicity while the ^{12}C component, hence the ^{13}C neutron source, in the intershell are of primary origin. In metal-deficient environments ([Fe/H] < −1), in proportion, more neutrons are available for each iron seed resulting in larger overabundances of heavy *s*-process elements with respect to lighter ones ([hs/ls]). However, to date no clear relation has been observed between [hs/ls] and metallicity (see e.g. Fig. 10 in van Aarle et al. 2011) in post-AGB stars. The end product of the *s*-process nucleosynthesis chain is the double magic lead ^{208}Pb isotope, which is predicted to have large overabundances with respect to other *s*-elements in metal-poor conditions (see Gallino et al. 1998; Goriely & Mowlavi 2000; and Lugaro et al. 2012, and references therein). The detection of metal-deficient objects with strong Pb enhancement by e.g. Van Eck et al. (2001, 2003) and Behara et al. (2010) confirm these predictions. However, some low-metallicity extrinsically *s*-process enriched objects (i.e. binaries) were found without strong Pb overabundance (Aoki et al. 2001; Van Eck et al. 2003). These are just a few illustrations that show that our understanding of the *s*-process nucleosynthesis is limited. Additional systematic observations are required to deduce *s*-process distributions, including Pb abundances, to improve our understanding of the third dredge-up and AGB nucleosynthesis mechanisms (e.g. Herwig 2005, and references therein).

In De Smedt et al. (2012, Paper I), we performed an extensive spectral abundance analysis of the Small Magellanic Cloud (SMC) post-AGB object J004441.04-732136.4 (hereafter abbreviated to J004441). As a 21 μm source (Volk et al. 2011),

⋆ Based on observations collected with the Very Large Telescope at the ESO Paranal Observatory (Chili) of programme number 084.D-0932 and 088.D-0433.

J004441 shows very strong *s*-process enhancement combined with a low metallicity of [Fe/H] = −1.34 ± 0.32 and a modest C/O ratio of 1.9 ± 0.7. A luminosity of 7600 ± 200 $L_{\odot}$ was derived with the known distance to the SMC. Comparison of the position of J00441 in the HR diagram to evolutionary post-AGB tracks of Vassiliadis & Wood (1994) resulted in an estimated initial mass of approximately 1.3 $M_{\odot}$. Based upon the initial mass and metallicity, different theoretical models were calculated with two independent stellar evolution codes, namely the Mount-Stromlo Evolutionary code (Karakas 2010, and references therein) and the STAREVOL code (e.g. Siess 2007, and references therein). The theoretical predictions match the *s*-process distribution but fail to reproduce the high overabundances and the modest C/O ratio. All models predict strong Pb overabundances but unfortunately, the strongest spectral Pb line at 4057.807 Å was only covered by a very low signal-to-noise (S/N) spectrum, preventing an accurate Pb abundance determination with the data of Paper I. We therefore reanalysed the Pb abundance of J004441 using a newly obtained UVES spectrum which is described in this Letter.

In addition, we determine upper limits for the Pb abundances for three Large Magellanic Cloud (LMC) post-AGB objects. Accurate spectral abundance studies of these objects have been conducted by van Aarle et al. (2011), but Pb was not included in their analysis. Comparison of the different Pb enhancements will provide insight into the intrinsic enrichment of metal-poor, low-mass AGB objects.

In the following section, we report on the new data and Sect. 3 describes our analysis and abundance determination. We compare the results of J004441 with model predictions in Sect. 4, followed by analyses of the Pb abundances for the LMC objects in Sect. 5. We end with a brief discussion.

2. Observations and data reduction

We use high-resolution spectra obtained with the UVES spectrograph (Dekker et al. 2000) mounted on the VLT. Apart from the UVES spectra used in Paper I, we obtained a new UVES spectrum with an exposure time of 1500 s. The dichroic beam splitter was used, which provided a wavelength coverage from approximately 3760 to 4985 Å for the blue arm and 6705 to 8513 Å and 8663 to 10 420 Å for the lower and upper parts of the mosaic CCD chip, respectively. This results in a wavelength range overlap with the Paper I spectra of 3760 to 4530 Å, 4780 to 4985 Å, and 6705 to 6810 Å.

Reduction of the UVES data is performed using the Reflex environment. In an attempt to optimize the S/N of the blue spectra, the new blue spectrum is reduced using different settings for the slit length and wavelength bin size in the reduction pipeline. Then the S/N of the different spectra are determined by computing the standard deviation obtained in different continuum regions in the wavelength range from 4800 Å to 4950 Å. This wavelength range is present in both the old and new spectra. For the new data, the best S/N was found for the standard parameter settings in the pipeline. Based upon the S/N results for the new data, the spectra of Paper I are also reduced again using the standard parameter settings in the pipeline.

The different blue spectra are then merged into a weighted mean spectrum. The weights are based upon the S/N quality. A small spectral window of 50 Å around the strongest 4057.807 Å Pb line is then normalized by fitting a fifth order polynomial through interactively defined continuum points. The final S/N of this combined spectrum is ∼25 in the region of the Pb line.

Table 1. Determined atmospheric parameters of J004441 in Paper I and three LMC objects of van Aarle et al. (2011).

	J004441	J050632	J052043	J053250
$T_{\rm eff}$ (K)	6250 ± 250	6750 ± 250	5750 ± 250	5500 ± 250
log g (dex)	0.5 ± 0.5	0.5 ± 0.5	0.0 ± 0.5	0.0 ± 0.5
$\xi_{\rm t}$ (km s^{-1})	3.5 ± 0.5	3.0 ± 0.5	3.0 ± 0.5	3.0 ± 0.5
[Fe/H] (dex)	−1.34 ± 0.32	−1.22 ± 0.18	−1.15 ± 0.20	−1.22 ± 0.19
$L/L_{\odot}$	7600 ± 200	5400 ± 700	8700 ± 1000	6500 ± 1000

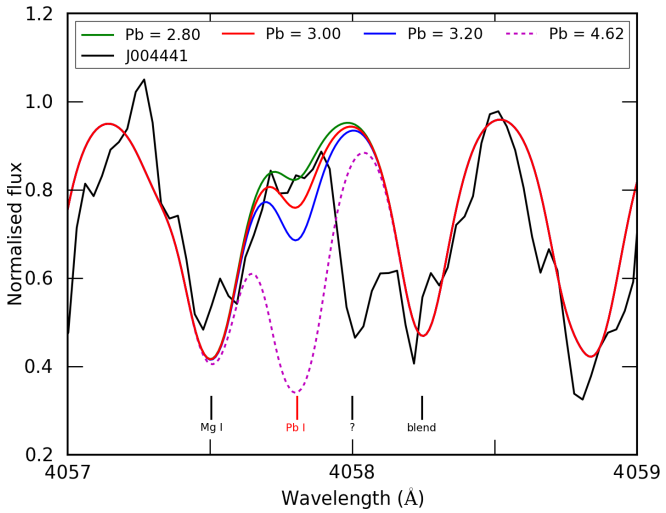

Fig. 1. Upper limit Pb abundance determination of J004441 using spectrum synthesis. The black spectrum is J004441 while coloured spectra represent synthetic spectra with different Pb abundances. Full coloured lines are used for the upper limit Pb abundance determination, the dashed magenta line represents the line when assuming an Pb abundance as predicted by the best fitting AGB model (see Sect. 4). The question mark indicates the position of an unidentified spectral line.

The velocity correction for the new data is exactly the same as for the previous data hence a heliocentric radial velocity of 148 ± 3 km s^{-1} is applied. This constant velocity suggests J004441 to be either a single star or a binary in a wide orbit.

3. Spectral analysis of Pb in J004441

For clarity, Table 1 shows the atmospheric parameters of J004441 (determined in Paper I), together with the derived parameters of three LMC objects from van Aarle et al. (2011), which is discussed below. We assume [Fe/H] as an accurate value of the mean metallicity of the stars. For all objects, we redid neither the atmospheric parameter determination nor the abundance analysis of already determined elements.

The merged spectrum quality is sufficient to determine an upper limit of the Pb abundance using the region around the 4057.807 Å line. We used an a local thermodynamical equilibrium (LTE) Kurucz-Castelli atmosphere model (Castelli & Kurucz 2003) with the atmospheric parameters shown in Table 1, combined with the LTE abundance calculation program MOOG (Sneden 1973) and VALD linelists (Kupka et al. 1999). The studied elemental abundances in Paper I, together with an overall metallicity [M/H] = −1.34 dex, are included in the spectral synthesis fit of the Pb line. Possible non-LTE effects are not taken into account.

Figure 1 displays the spectral synthesis fits to the Pb line in J004441. The coloured spectra represent different abundance values for Pb with all other elemental abundances constant. The

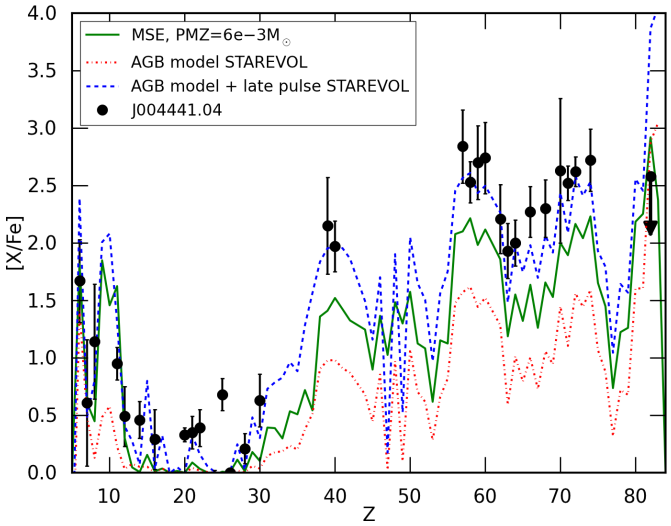

Fig. 2. Comparison of the J004441 abundance ratios with model predictions. Black dots represent the [*X*/Fe] results of J004441, the green line represents the Mount Stromlo (MSE) model, red and blue dashed lines show STAREVOL code predictions with the latter including a late thermal pulse with a deep dredge-up when dilution is small. The [Pb/Fe] result is indicated with a down arrow, representing an upper limit.

upper limit for the Pb abundance is derived by comparison with the full coloured lines. It is difficult to determine the continuum level accurately. The fit of the Mg I line to the left of the Pb line and the blended line at 4058.2 Å are used as estimates of the continuum position. The question mark in Fig. 1, indicates the wavelength position of a spectral line which remains unidentified despite our efforts. Manually increasing the input abundance of all available elements in the region of this line did not change the synthetic spectrum, so we conclude that this line is not present in the VALD linelist. In strongly *s*-process enhanced photospheres, the mere line identification is often problematic (e.g. Reyniers et al. 2002). Considering the strong *s*-process enrichment of J004441, this line is probably an unidentified *s*-process spectral line. The identification of this spectral line is essential for constraining a more accurate Pb abundance, and it allows us to set an upper limit for the Pb abundance around $\log_\epsilon$ (Pb) = 3.0 ($\log_\epsilon$ (H) = 12.0).

To test the abundance fit, we replaced the VALD Pb line in the VALD linelist by the analogue Pb line from the NIST Atomic Spectra Database (Kramida et al. 2013) and the Pb line analogue from the Pb line list used in Van Eck et al. (2003). The oscillator strengths ($\log gf$) for the VALD, NIST, and Van Eck linelists for the Pb line are −0.17 dex, −0.18 dex and −0.22 dex, respectively, while the excitation potential is 1.32 eV for all linelists. This results in a maximal abundance difference of 0.05 dex, which is neglible with respect to the uncertainty due to the continuum position. Also the isotopic Pb line list of Van Eck et al. (2003) was fitted assuming solar isotope ratios and obviously resulted in an even lower Pb abundance upper limit, which seems improbable considering the Pb abundance discrepancy in Sect. 4. We therefore adopt a Pb abundance of $\log_\epsilon$(Pb) = 3.0 for comparison with AGB models.

The nitrogen (N) abundance is also derived using spectral synthesis. In Paper I, no clear N lines were detected in the optical part of the spectra. However, the new spectra cover a wider wavelength range towards the IR, displaying clear unblended N lines. Based upon the analysis of five spectral lines, we find $\log_\epsilon$ (N) = 7.10 ± 0.32 where the error contains model, line-to-line scatter, and non-LTE uncertainties. We apply a non-LTE correction of 0.3 dex as found in Lyubimkov et al. (2011) to similar objects and adopt this value as the non-LTE uncertainty.

Table 2. [*s*/Fe] results for specific *s*-elements of the studied objects.

	[La/Fe]	[Ce/Fe]	[Nd/Fe]	[Pb/Fe]
J004441	2.84 ± 0.32	2.53 ± 0.18	2.74 ± 0.31	<2.58
J050632	1.48 ± 0.25	1.33 ± 0.23	1.18 ± 0.31	<1.52
J052043	1.85 ± 0.24	1.68 ± 0.20	1.92 ± 0.26	<1.40
J053250	2.03 ± 0.26	1.91 ± 0.20	2.02 ± 0.24	<1.70

4. AGB chemical models

We compare the newly derived abundance results with model predictions from two independent stellar evolution codes of Paper I. Both codes calculated models for a 1.3 $M_\odot$ star of [Fe/H] = −1.4 for which the calculated AGB tip luminosities are somewhat higher than the observed luminosity. The luminosities can be fine-tuned by increasing the mass-loss rate, but this should not alter the predicted abundance profiles.

The observed abundances compared to model predictions are shown in Fig. 2 where different coloured lines represent different model predictions. The derived [Pb/Fe] upper limit of J004441 is indicated with a down arrow. The Mount-Stromlo Evolutionary (MSE) predictions (Karakas 2010, and references therein) are calculated for a metallicity of Z = 0.0006, while both STAREVOL code predictions (e.g. Siess 2007, and references therein) have a reference composition of Z = 0.0044 (see Paper I) and are calculated using the same parameter values. The red STAREVOL model in includes a late thermal pulse combined with a deep dredge-up, resulting in substantial surface pollution due to the low convective envelope mass. A detailed description of the conclusions drawn from Fig. 2 for C, O, and *s*-elements except Pb, is given in Paper I and will not be repeated in this Letter.

The dashed magenta line in Fig. 1 is computed using the [Pb/Fe] = 4.62 as predicted from the best fitting AGB model in Fig. 2 and clearly shows that such a high Pb abundance is incompatible with our spectrum. Figure 2 also indicates that the Pb overabundance is similar to that of the other heavy *s*-process peak elements (La, Ce and Nd around Z = 60). The newly derived N abundance (Z = 7) fits the different model predictions well.

5. LMC objects

To expand the sample of studied Pb abundances in *s*-process enriched post-AGB stars, Pb abundance upper limits are derived for three LMC objects studied by van Aarle et al. (2011, Paper II). These three objects are J050632.10-714229.8, J052043.86-692341.0, and J053250.69-713925.8, hereafter respectively abbreviated to J050632, J052043, and J053250. For the Pb abundance analysis, we use the normalized spectra of Paper II. For J052043, two studies were conducted in Paper II of which we use the spectra observed in December (J052043_b in Paper II). Table 1 shows the atmospheric parameters of the three objects. All objects are found to be metal-poor and to have initial masses below 1.5 $M_\odot$. In none of the objects is the Pb line clearly detected.

Similar to the study of J004441, spectral synthesis is used for the Pb abundance determinations of the three LMC objects.

Table 2 lists the [*s*/Fe] determinations for Ba-peak elements, along with the Pb abundance upper limits. The shown abundance results of the three LMC objects are derived in Paper II, except for Pb. For none of the objects is the [Pb/Fe] uncertainty larger than 0.08 dex due to model uncertainties. The [*s*/Fe] results for all studied *s*-elements of the different objects are shown in the upper panel of Fig. 3. For a given metallicity, the overabundances depend on the amount of dilution in the envelope mass. Therefore, the lower panel of Fig. 3 shows the [*s*/Fe] results scaled to [La/Fe] of J052043 to show the *s*-process distribution of the different stars independent of dilution. From Table 2 and Fig. 3, we conclude that for J004441 and J050632, the Pb upper limit overabundance is similar to the overabundances of the Ba-peak elements, while for J052043 and J053250, Pb is modestly underabundant with respect to Ba-peak elements.

6. Discussion and conclusion

Using additional spectra of J004441, an *s*-process rich post-AGB star in the SMC, we obtained an upper limit of the Pb abundance. With [Pb/Fe] < 2.58, Pb shows a similar or smaller overabundance than the *s*-process elements of the Ba-peak. However, this upper limit is much smaller than predicted by our specific AGB models. The latter were tuned to the initial mass and metallicity of the object and focussed on a fit through the obtained overabundances of the Zr- and Ba-peak elements. This discrepancy is real and not due to the poor S/N of the spectrum. The *s*-process predictions of the tuned AGB models, based on successive thermal pulses with associated partial mixing and dredge-ups are not able to reproduce the low Pb abundance.

The [Pb/Fe] results for the three LMC objects are similar to J004441: there is no predicted high Pb overabundance relative to the Ba-peak elements. Although having a strong *s*-process enrichment, the four low-mass, metal-deficient post-AGB stars of the Magellanic clouds all show the absence of the theoretically predicted strong Pb overabundances. This trend is similar to what is observed in some, but not all, extrinsically enriched objects in Aoki et al. (2001) and Van Eck et al. (2003). Current AGB models based on a ^{13}C-pocket arising from diffusive overshooting at the base of the convective envelope during the third dredge-up have problems reproducing the observed low Pb abundances in metal poor stars, the spread in [hs/ls] at a given metallicity and/or the C/O ratios. This clearly indicates that some physical ingredients are missing in the description of this process. To improve the situation, we need to obtain full abundance patterns of many post-AGB stars in both the LMC and SMC, so that we can identify systematics in the observed patterns. Simultaneously, we need to explore alternative processes to explain the derived abundance profiles. In this study, we used the diffusive approach to form the ^{13}C pocket, but the partial mixing of protons below the envelope may not be diffusive in essence but rather advective. For instance, when adopting a new mixing algorithm, Straniero et al. (2006) were able to generate a more massive ^{13}C pocket and consequently produce higher *s*-process surface enrichments in better agreement with observations. Rotation is also a key physical ingredient that may have a strong impact on the synthesis of *s*-elements. Depending on the degree of shear, the *s*-process nucleosynthesis can be completely inhibited (see e.g. Langer et al. 1999; Herwig et al. 2003; Siess et al. 2004) or partially activated (Piersanti et al. 2013).

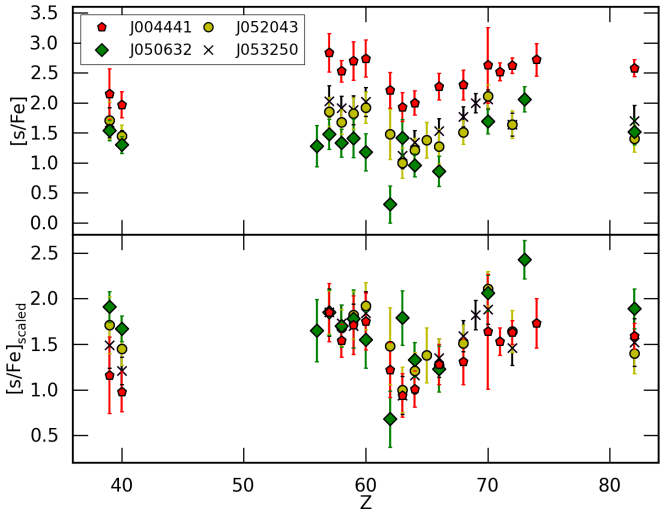

Fig. 3. *Upper panel*: overview of [*s*/Fe] for the different objects. The values at $Z = 82$ represent the derived Pb abundance upper limits. *Lower panel*: [*s*/Fe] for the different objects scaled to [La/Fe] at $Z = 57$.

Also the effect of internal gravity wave mixing (Denissenkov & Tout 2003) on the *s*-process nucleosynthesis still needs to be explored.

Additional work, both theoretically assisted by direct hydrodynamical simulations and observational with systematic abundance determinations of a whole population of post-AGB stars with well constrained distances and a spread in metallicity, is needed to better constrain the *s*-process mechanisms.

References

Abia, C., Domínguez, I., Gallino, R., et al. 2002, ApJ, 579, 817
Aoki, W., Ryan, S. G., Norris, J. E., et al. 2001, ApJ, 561, 346
Behara, N. T., Bonifacio, P., Ludwig, H.-G., et al. 2010, A&A, 513, A72
Castelli, F., & Kurucz, R. L. 2003, in Proc. IAU Symp. 210, Poster A20
De Smedt, K., Van Winckel, H., Karakas, A. I., et al. 2012, A&A, 541, A67
Dekker, H., D'Odorico, S., Kaufer, A., Delabre, B., & Kotzlowski, H. 2000, in SPIE Conf. Ser. 4008, eds. M. Iye, & A. F. Moorwood, 534
Denissenkov, P. A., & Tout, C. A. 2003, MNRAS, 340, 722
Gallino, R., Arlandini, C., Busso, M., et al. 1998, ApJ, 497, 388
Goriely, S., & Mowlavi, N. 2000, A&A, 362, 599
Herwig, F. 2005, ARA&A, 43, 435
Herwig, F., Langer, N., & Lugaro, M. 2003, ApJ, 593, 1056
Karakas, A. I. 2010, MNRAS, 403, 1413
Kramida, A., Ralchenko, Yu., Reader, J., & NIST ASD Team 2013, NIST Atomic Spectra Database, v.5.1, http://physics.nist.gov/asd, National Institute of Standards and Technology, Gaithersburg, MD
Kupka, F., Piskunov, N., Ryabchikova, T. A., Stempels, H. C., & Weiss, W. W. 1999, A&AS, 138, 119
Langer, N., Heger, A., Wellstein, S., & Herwig, F. 1999, A&A, 346, L37
Lugaro, M., Karakas, A. I., Stancliffe, R. J., & Rijs, C. 2012, ApJ, 747, 2
Lyubimkov, L. S., Lambert, D. L., Korotin, S. A., et al. 2011, MNRAS, 410, 1774
Piersanti, L., Cristallo, S., & Straniero, O. 2013, ApJ, 774, 98
Reyniers, M., Van Winckel, H., Biémont, E., & Quinet, P. 2002, A&A, 395, L35
Siess, L. 2007, A&A, 476, 893
Siess, L., Goriely, S., & Langer, N. 2004, A&A, 415, 1089
Sneden, C. A. 1973, Ph.D. thesis, The Univerisity of Texas at Austin
Straniero, O., Gallino, R., Busso, M., et al. 1995, ApJ, 440, L85
Straniero, O., Gallino, R., & Cristallo, S. 2006, Nucl. Phys. A, 777, 311
van Aarle, E., van Winckel, H., Lloyd Evans, T., et al. 2011, A&A, 530, A90
Van Eck, S., Goriely, S., Jorissen, A., & Plez, B. 2001, Nature, 412, 793
Van Eck, S., Goriely, S., Jorissen, A., & Plez, B. 2003, A&A, 404, 291
Vassiliadis, E., & Wood, P. R. 1994, ApJS, 92, 125
Volk, K., Hrivnak, B. J., Matsuura, M., et al. 2011, ApJ, 735, 127